Unlocking rock properties using viscoelastic multiparameter FWI

James McLeman[1], Jennifer Badry[2], Tom Rayment[1], and Alex Pauli[2]

https://doi.org/10.1190/tle-2025-1055

Abstract

Conventional imaging methods like reverse-time migration impose assumptions, such as the Born approximation, that introduce strict data preprocessing requirements, which reduce their effectiveness in regions of strong impedance contrasts, complex structural geometries, and poor illumination. Multiparameter full-waveform inversion (MP-FWI) offers an alternative approach that enables the simultaneous estimation of many subsurface properties (e.g., V_P and reflectivity) directly from raw seismic data. MP-FWI is a least-squares solution that uses the full wavefield, treating multiples as valuable signals to improve resolution and illumination. In recent years, MP-FWI approaches have assumed acoustic wave propagation to generate angle-dependent reflectivity for elastic amplitude-versus-angle (AVA) analysis, which enables P-impedance and V_S/V_P ratio estimation via an additional inversion step. Elastic MP-FWI offers the potential to skip this additional inversion step and determine these AVA attributes directly from the acquired data. In this article, two case studies from the Australian North West Shelf and the Gulf of Mexico are presented, demonstrating the fidelity of viscoelastic MP-FWI in deriving AVA attributes. The accuracy of these inverted models is evaluated against the conventional workflow and well data, and the role of quantitative interpretation expertise is discussed in the context of this novel paradigm.

Introduction

Hydrocarbon reservoir characterization has relied on amplitude-versus-angle (AVA) attributes obtained from seismic data processing and imaging for decades. Conventional workflows to derive such AVA attributes typically consist of four key stages: preprocessing, model building, imaging (migration), and AVA inversion. The model-building stage aims to build background (low-wavenumber) velocity, anisotropy, and Q-models (attenuation), which are then used in the imaging/migration stage to generate prestack reflectivity from the preprocessed seismic data. AVA attributes, such as V_P/V_S ratio and P-impedance, can then be determined using the prestack reflectivity amplitudes in the AVA-inversion stage (Zoeppritz, 1919; Aki and Richards, 2002). Although each stage has been extensively refined and optimized over the years, the overall structure of it has changed very little. This is due to the assumptions and approximations embedded in the latter imaging and AVA-inversion stages, requiring data inputs that meet these requirements, motivating the former stages of preprocessing and model building.

Conventional imaging algorithms, such as Kirchhoff prestack depth migration (Audebert et al., 1997; Bleistein et al., 2001) and reverse-time migration (RTM) (Baysal et al., 1983; Bednar et al., 2003), rely on a plethora of assumptions about the earth, such as the acoustic and single-scattering (Born) approximation. These necessitate data inputs, which have attenuated parts of the recorded wavefield that do not agree with these assumptions, such as ghosts and multiples. Such multiscattering arrivals contain valuable information about the subsurface that is unfortunately discarded in such approaches. This limits the subsurface illumination to primary-only reflections, which can be limited in the near surface of shallow water environments or in complex geology such as (pre-)salt. Although the least-squares imaging extensions of such techniques (Nemeth et al., 1999; Guitton, 2017) enhance amplitude fidelity and improve subsurface illumination compensation, their assumptions are still limiting factors in regions with high-impedance contrasts or complex geology.

Full-waveform inversion (FWI) (Tarantola, 1986) offers an alternative approach to determining AVA attributes because it directly inverts for the subsurface properties with the capability of using the full wavefield, which includes multiples, ghosts, and transmission arrivals. Unlike the conventional imaging approaches, FWI treats multiples as valuable information that can improve illumination and resolution. However, due to computational costs, it has historically been used to invert for V_P using only diving waves at low frequency under the acoustic approximation, making it an additional tool for the model-building stage instead of realizing its full potential. In recent years, acoustic FWI has evolved into a high-frequency imaging tool that incorporates reflections when inverting for V_P, which can aid structural interpretation either in its own right or through its subsequent spatial derivatives, commonly known as FWI-derived reflectivity (Shen et al., 2018; Kalinicheva et al., 2020). It has been common with these approaches to assume a simple relationship between V_P and density, such as Gardner's relation (Gardner et al., 1974). This type of relationship, however, can often prove unreliable in many common geologic settings, such as in unconsolidated shallow sediments or shales (Sayers and den Boer, 2011). Similar observations can be made about the Greenberg–Castagna relation for V_P and V_S. Inaccuracies in such assumptions will translate into errors

Manuscript received 10 December 2025; revision received 18 February 2026; accepted 31 March 2026; published ahead of production 19 April 2026.

[1]DUG Technology (UK), London, UK. E-mail: jamesm@dug.com; tomr@dug.com.
[2]DUG Technology (Australia), West Perth, Western Australia, Australia. E-mail: jenniferb@dug.com; alexp@dug.com.

in the inverted models, which can result in unreliable amplitudes in the derived reflectivity. The common use of amplitude normalization schemes and amplitude-insensitive objective functions, such as those based on cross-correlation time shifts (Luo and Schuster, 1991), also renders the amplitude fidelity of such results questionable.

Multiparameter FWI (MP-FWI) imaging approaches (McLeman et al., 2023) simultaneously determine additional subsurface properties (such as P-impedance, anisotropy, and Q) directly from raw seismic data without assuming relations between the inverted parameters. Industrial-scale MP-FWI applications have traditionally relied on the acoustic-wave assumption, which generates robust angle-dependent reflectivity for AVA analysis using the full wavefield to determine quantities, such as intercept, gradient, or subsequent properties, via rotation through the chi angle (Hidalgo et al., 2024). Subsequent elastic properties, such as P-impedance and V_P/V_S ratio, can be obtained via an additional step of conventional AVA inversion (Warner et al., 2022; McLeman et al., 2023). Thus, acoustic MP-FWI has demonstrated the capability to replace the conventional four-stage workflow with a simpler two-stage workflow: MP-FWI for angle-dependent reflectivity and then AVA inversion. This simplification avoids the need for extensive data preprocessing workflows, which can contain a multitude of steps such as deghosting, designature, demultiple, and regularization that are time-consuming to test and require many subjective judgments that affect the quality of the final result.

The ever-increasing geologic complexity in which hydrocarbon reservoirs are identified can also cause the acoustic approximation to become severely abused and has driven the development of imaging technologies into the elastic and viscoelastic regime to produce high-resolution AVA attributes to reduce exploration and production risk (Köhn et al., 2009; Yuan et al., 2015; Pan et al., 2018). With advances in high-performance computing, running 3D elastic MP-FWI at the resolution required for quantitative interpretation (QI) (Wang et al., 2021; Baumstein et al., 2022; Shen et al., 2024; Gomes et al., 2025) has become feasible, enabling the estimation of quantities such as P-impedance and V_P/V_S ratio from raw (or minimally processed) field data without requiring the secondary AVA-inversion step. This avoids the need to generate angle-dependent reflectivity. Elastic MP-FWI offers the opportunity to simultaneously resolve not only the subsurface structural features but also accurate AVA-attribute information. Figure 1 shows a comparison of the conventional workflow, acoustic MP-FWI workflow, and elastic MP-FWI workflow to derive elastic AVA attributes from field data.

In this work, we present two case studies that evaluate the fidelity of high-frequency viscoelastic MP-FWI-derived AVA attributes. The first extends the work of McLeman et al. (2023) using a towed-streamer seismic data set from the Australian North West Shelf. The second case study considers an ocean-bottom node (OBN) data set from the Gulf of Mexico (GoM). The results are compared with well-log data and evaluated against the conventional workflow approach.

Case study: Australian North West Shelf

This first case study is from the Australian North West Shelf, located approximately 115 km northwest of Barrow Island, near the Gorgon Gas Field in the offshore Carnarvon Basin. This region contains rapidly changing shallow velocity variations due to localized channel features and carbonates. The primary objectives were in the late Triassic sandstones of the upper Mungaroo Formation, which contain large gas reserves, where all of the target reservoirs have strong AVA signatures. The seismic data acquisition took place in 2006 using a narrow-azimuth dual-source marine towed-streamer with 8 cables and a maximum offset of 6 km. The streamer only measured pressure using hydrophone receivers.

The initial V_P model was built using a smoothed existing regional model that was refined with diving wave-only acoustic FWI in steps of increasing frequency up to a bandwidth of 0–19 Hz. Note that the lower bound of 0 Hz is written to reflect the fact that we did not explicitly apply a low-cut filter as part of FWI; however, bandwidth limitations of the physical sources and receivers meant that the observed data had a poor signal-to-noise ratio below 5 Hz. The relatively short maximum offset available restricted the update depth using the diving waves to approximately 2 km. Initial low-frequency models for the V_S/V_P ratio, density, and anisotropy were built using well data available in the survey area, regional knowledge, and extrapolation along structural horizons.

These initial models were input to viscoelastic MP-FWI, simultaneously updating V_P and P-impedance at 0–11, 0–14, and 0–19 Hz using reflections and the inversion method described in McLeman et al., 2023. For this two-parameter update, no partition in the data domain was performed to separate near and far angles. This initial stage proved beneficial to refine the V_P update at lower frequencies to avoid cycle skipping before inverting for the V_S/V_P ratio. The purpose of the simultaneous P-impedance and V_P update at this stage was to use the reflections to update both parameters while reducing density leakage into V_P. Significant V_P changes meant that anisotropy was then updated from 0 to 19 Hz, and the P-impedance was further refined using a single-parameter FWI, where only the near reflection angles were considered because their amplitudes are mostly dependent on P-impedance (Wang et al., 2021). With V_P and P-impedance models being well established, viscoelastic MP-FWI was then used to simultaneously invert for V_P, V_S/V_P ratio, and P-impedance using all reflection angles with the frequency steps of 0–19, 0–27, 0–35, and finally 0–60 Hz. The only model domain constraints applied to V_S/V_P were clip constraints aimed at preventing nonphysical values. During the inversion stages, no relationships between the inverted parameters were assumed or enforced as constraints. A least-squares objective function was used during viscoelastic MP-FWI updates, and raw hydrophone field data were used as input.

The design of this approach aimed to reduce the cross-talk between the three inverted parameters by taking advantage of the scattering patterns and corresponding wavenumber

sensitivities of the chosen inverted model parameterization (Gomes et al., 2025) and reducing the problem complexity by inverting parameters with different parts of the data. The crosstalk was further reduced using an L-BFGS optimizer with an adaptive gradient-like approach to better estimate the inverse Hessian (McLeman et al., 2023). To enable a significant computational cost reduction, we observe that this data set is hydrophone-only marine-towed streamer, and thus, we assume that the background V_S contributes less significantly than the background V_P. Therefore, we build the wavefield propagation grid that enables accurate modeling of P-wave kinematics and dynamics (Wang et al., 2021).

The source wavelet was derived using a modeled signature based on gun-array information and further refined via source inversion within FWI; near-field hydrophone data were not available for this acquisition, but would have been the preferred choice.

A second workflow was run for comparison purposes to generate a conventional processing and imaging result using designature, deghosting, demultiple, and 0–60 Hz viscoacoustic LS-RTM and Kirchhoff migration angle stacks. The input models to LS-RTM were the output models from the 0–60 Hz viscoelastic MP-FWI. Tidal variations were accounted for in the wave equation modeling for both workflows.

It is important to highlight that the data processing workflows needed to generate the inputs for these two imaging approaches are very different. In the LS-RTM case, designature, deghosting, and demultiple were applied, whereas for the viscoelastic MP-FWI approach, the raw field data was used in this case study. The reason this can be done is that the wave equation modeling engine in viscoelastic MP-FWI can correctly account for the effects of the free surface and internal multiples. Additional considerations such as tidal variations, water velocity variations, source and receiver array effects, and even water layer currents (Hampson, 2024) can also be included as part of the wave equation modeling for MP-FWI and LS-RTM, and so, corrections to the input data for these phenomena are not required. Such considerations become increasingly important at higher frequency. Although some of these considerations are useful in LS-RTM to achieve improved results, they are critical in MP-FWI because it must predict the full scattering series. Many conventional input-data corrections are adequate for primaries but not for multiples. Implementing these corrections (or ignoring the physics of these considerations entirely) will result in mismodeling of the multiples leading to multiple leakage and the reduced ability to use multiples in the construction of the final image. This is also true of Q effects, which must be included in the wave-equation modeling, hence the use of "visco" modeling operators.

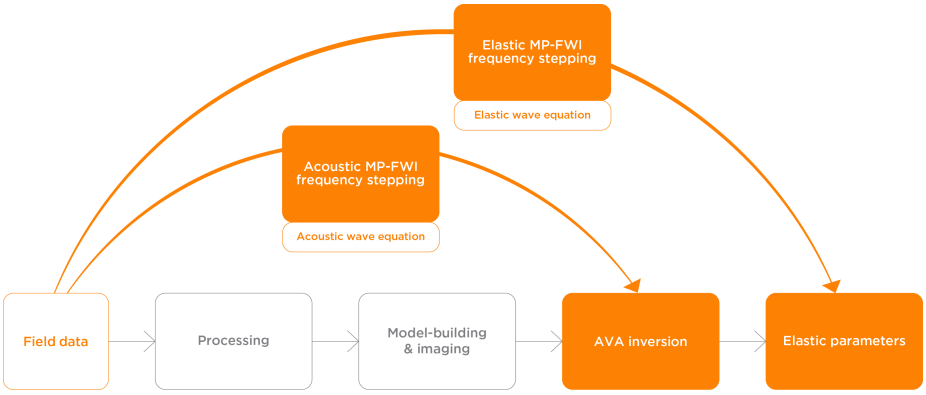

Figure 1. A schematic diagram showing a comparison of the conventional workflow (bottom), acoustic MP-FWI workflow (middle), and elastic MP-FWI workflow (top) to derive elastic AVA attributes from field data.

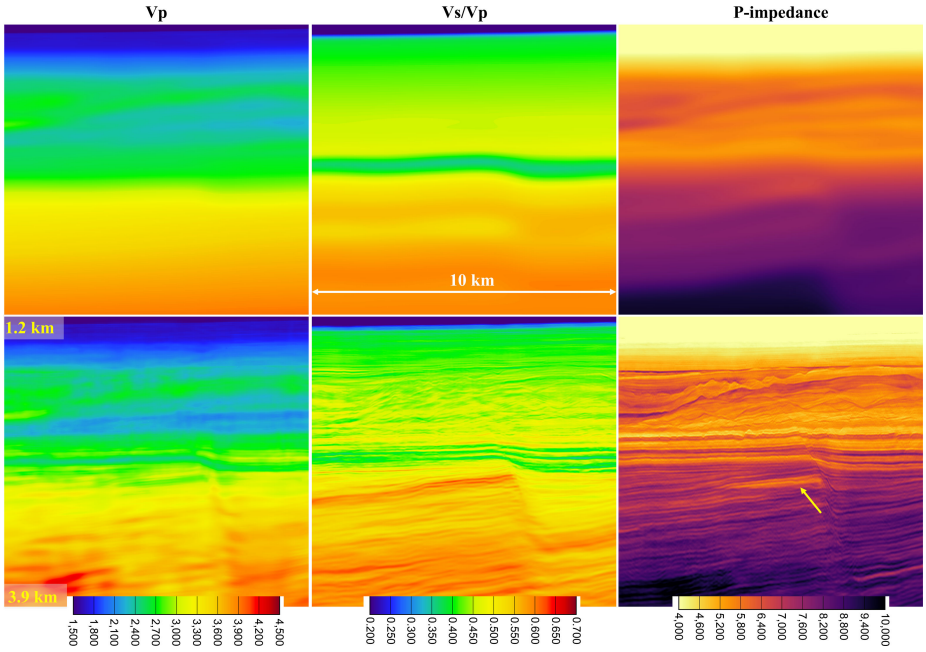

Figure 2. (Top) I_P, I_S/I_P, and P-impedance models input to viscoelastic MP-FWI and (bottom) the results after the 0–60 Hz viscoelastic MP-FWI workflow. The yellow arrow highlights the gas reservoir.

In Figure 2, a comparison is shown through an inline at the well location between the initial models and the models inverted by viscoelastic MP-FWI of P-impedance, V_S/V_P ratio, and V_P. The updated models demonstrate an increase in spatial resolution, with the thin layers becoming well delineated. We can also readily identify the hydrocarbon reservoir location in the updated models, as highlighted by the yellow arrow. At this location, we

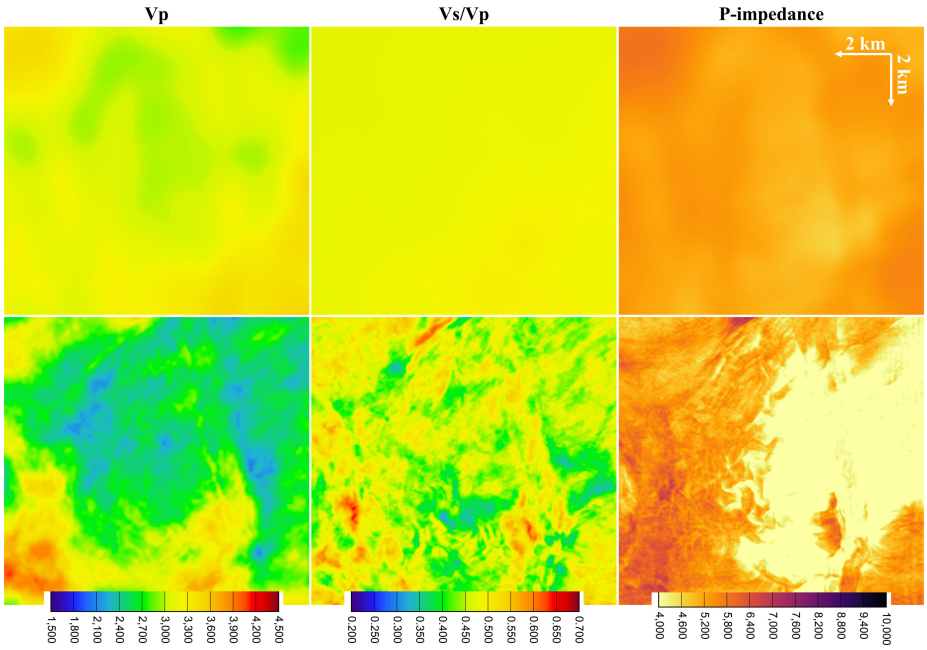

Figure 3. Depth slices through I_P, I_S/I_P, and P-impedance for (top) models input to viscoelastic MP-FWI and (bottom) the results after the 0–60 Hz viscoelastic MP-FWI workflow.

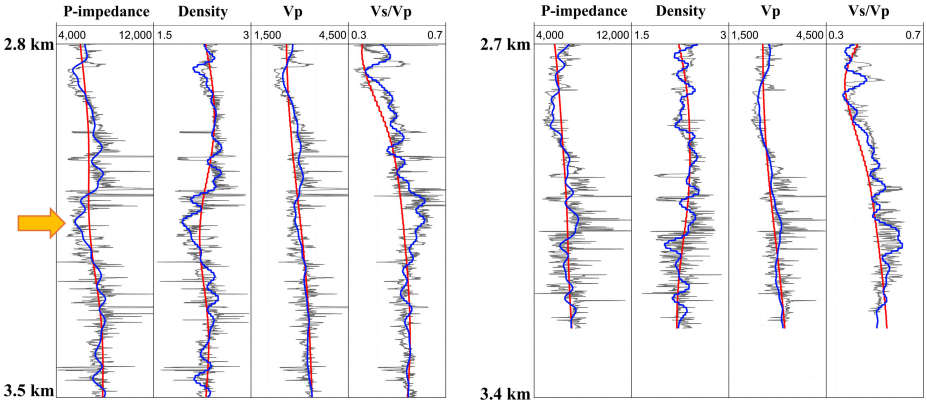

Figure 4. Comparison between the well information (black), the initial models input to viscoelastic MP-FWI (red), and the models inverted by viscoelastic MP-FWI (blue).

see a decrease in V_P due to the gas saturation of the rock, where such gas saturation will have minimal impact on V_S, causing the V_S/V_P ratio to increase. Gas saturation will cause a decrease in density as well as V_P, meaning the P-impedance should also decrease, and indeed, this is observed. A depth slice through these results is shown in Figure 3, which demonstrates the increase in spatial resolution brought by the viscoelastic MP-FWI approach.

To validate these results, these updated models are compared with the well logs. Well information from two wells within the survey area is shown in Figure 4 (black), where the viscoelastic MP-FWI initial models are shown in red, and the updated models are shown in blue. The orange arrow indicates a location where the well data show a decrease in P-impedance driven by a decrease in density and by a decrease in V_P, but the V_S/V_P ratio is predicted to increase. This shows that the viscoelastic MP-FWI updated models correctly predict these trends, demonstrating that the crosstalk between these parameters has been successfully mitigated. The well information was only used to build the initial low-frequency models and was not used as a constraint to guide the viscoelastic MP-FWI.

The amplitudes of the Kirchhoff migration angle stacks were inverted using a 3-term Aki–Richards approximation to obtain estimates of P-impedance and V_S/V_P ratio. This is shown in Figure 5, where the conventionally derived results are shown in red, the viscoelastic MP-FWI inverted models are shown in blue, and the well information is shown in yellow, with the gamma ray log shown in orange. A better match is observed between the viscoelastic MP-FWI derived models and the well information. This figure also shows the crossplots obtained from the two approaches, where the ellipses are modeled from the expected distribution of points based on the well logs. In the cross plot, the lithology beneath the gas sands is predicted to be brine sands, and above the reservoir is predicted to be shales, and indeed, this is what was found when drilling. However, we can see that although the distribution of points in the crossplot from the conventional approach does broadly match the modeled ellipses, they are not tightly clustered, likely due to the influence of noise in the AVA inversion. Comparing this to the viscoelastic MP-FWI result, it is evident that the reservoir is much better delineated, and we can see that the distribution of points in the modeled ellipses is more tightly clustered and better shows the expected trends, giving more confidence in the result.

An important aspect to highlight about these results is that they are absolute quantities, not relative quantities. Seismic data and the wave equation are generally insensitive to low-wavenumber changes in density, and so, without the use of a priori information, such as well logs, the inverted density represents a relative quantity. When inverting for hydrophone-only seismic data, a similar story can be found for low-wavenumber V_S, but to a lesser extent because the presence of converted waves (e.g., a PSSP arrival) means that their kinematics could be used to build a low-wavenumber V_S. However, the tomographic V_S term tends to be weak when inverting for hydrophone-only data, making low-wavenumber V_S updates challenging. The use of well data and the expertise of a QI specialist were critical

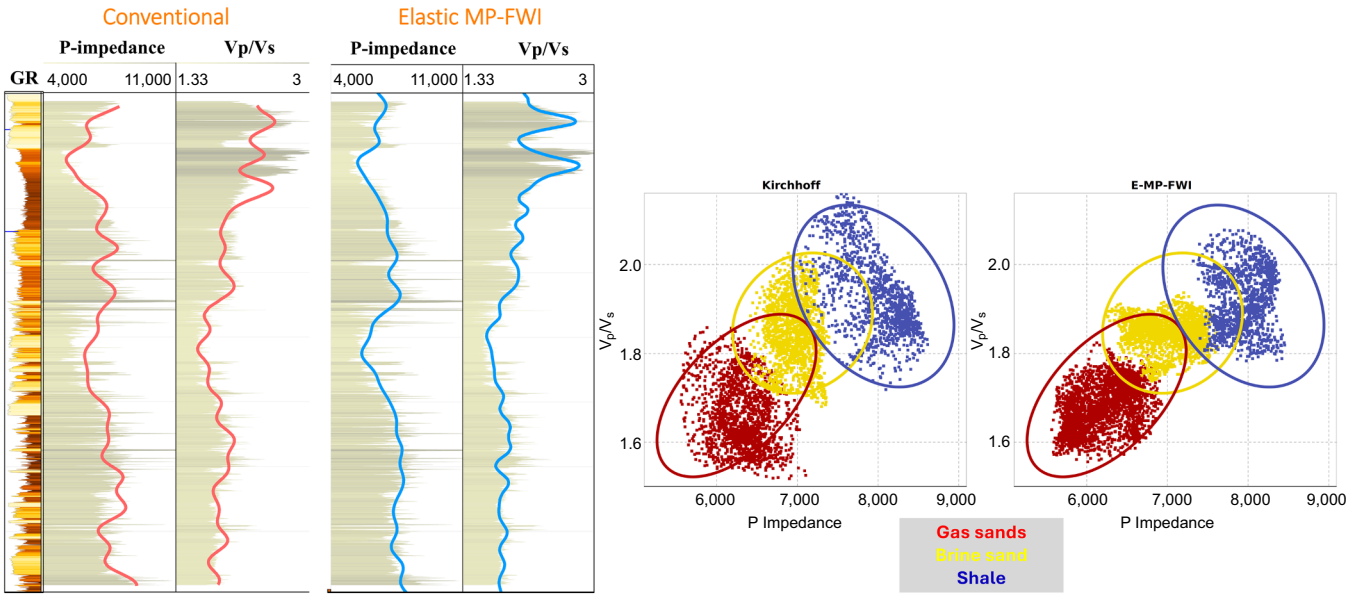

Figure 5. Comparison between the well information (with gamma ray log) (yellow), the Kirchhoff migration result (red), and the models obtained from viscoelastic MP-FWI (blue). The corresponding crossplots are shown on the right-hand side.

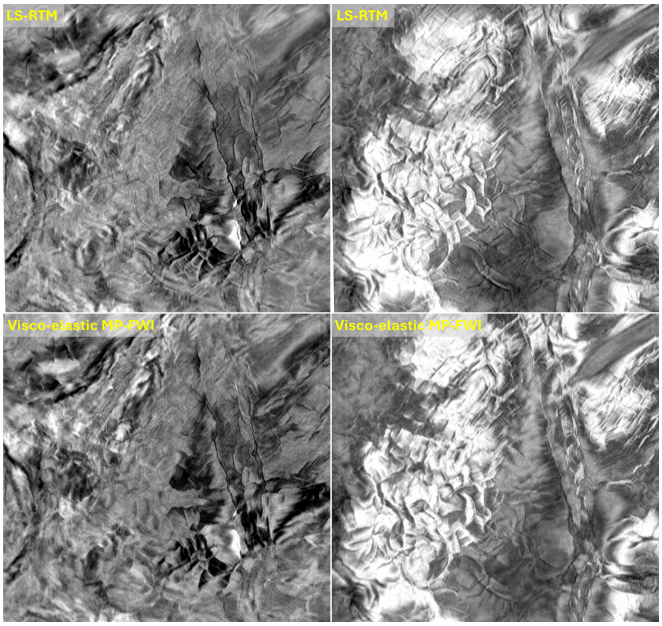

Figure 6. (Top) LS-RTM depth slices at 2480 and 2570 m and (bottom) the equivalent viscoelastic MP-FWI depth slices.

throughout the viscoelastic MP-FWI workflow to ensure that the results represented an absolute rather than a relative quantity. In exploration regions where well data are not available, additional sensor measurements, such as multicomponent OBN, could be used to build a low-wavenumber V_S model from the surface waves and horizontal particle velocity measurements (Masmoudi et al., 2024). The inclusion of gravity data measurements could be a potential (pun intended) opportunity to be used to build a low-wavenumber density model instead (Jiang, 2020; Liu et al., 2024).

The reflectivity derived from viscoelastic MP-FWI is obtained by considering the vertical spatial derivative of the natural logarithm of P-impedance and is shown in Figure 6 with a depth slice at 2480 and 2570 m in comparison to the reflectivity generated by the LS-RTM. It is important to highlight that the viscoelastic MP-FWI results used the raw unprocessed shots as input, whereas the LS-RTM used highly preprocessed input data. The reflectivity generated by viscoelastic MP-FWI demonstrates an increase in spatial resolution over the viscoacoustic LS-RTM, where the subsurface channel features and complex faulting are sharper and more clearly delineated.

Case study: Gulf of Mexico

In this second case study, a sparse OBN data set acquired in the GoM is considered, in a region where the water depths are approximately 2 km. The initial low-wavenumber models of density, anisotropy, and V_S/V_P ratio were derived using regional knowledge and well data and were extrapolated along structural horizons. In a similar fashion to the previous case study, the expertise of a QI specialist was crucial in building the initial low-wavenumber models to ensure that the final inversion result represents an absolute quantity.

Viscoelastic MP-FWI (with reflections) was performed in increasing frequency bands of 0–6, 0–9, 0–14, 0–20, and 0–30 Hz. It began by jointly inverting for P-impedance and V_P while keeping the V_S/V_P ratio fixed. The updated P-impedance volume was then carried into further passes of viscoelastic MP-FWI, in which P-impedance, the V_S/V_P ratio, and V_P were updated simultaneously. As in the previous case study, the strategy was to mitigate parameter crosstalk by breaking the inversion problem into smaller pieces, where selected combinations of parameters with each step were solved for. The chosen parameterization (P-impedance, V_S/V_P, and V_P) together with the same optimization approach was again used to further limit crosstalk.

The input seismic data for the viscoelastic MP-FWI underwent minimal preprocessing, notably node repositioning

guided by direct-arrival analysis. For this case study, only the hydrophone data were used. In parallel, a standard preprocessing flow was applied to produce data for a downgoing-mirror RTM using the velocity model derived from the viscoelastic MP-FWI.

A comparison of the viscoelastic MP-FWI inverted parameters at a well location is shown in Figure 7. The initial models input to MP-FWI are shown in red, the inverted models are in blue, and the well data are in black. We observe a good match between the inverted P-impedance, V_S, density, and V_P with the well data.

A structural comparison of the downgoing mirror RTM using preprocessed data, the viscoacoustic MP-FWI-derived reflectivity, and the viscoelastic MP-FWI-derived reflectivity can be found in Figure 8. The improvements that MP-FWI can bring over the conventional RTM are readily identifiable due to the inclusion of the multiscattered energy, with the unrealistic amplitude variations being resolved by the least-squares nature of the approach, resulting in an improvement in illumination and resolution. Further improvements in focusing around the high-impedance contrast given by the salt are highlighted in the viscoelastic MP-FWI-derived reflectivity result, and subsequently, the structures beneath it in the presalt demonstrate an improvement in focusing too, as highlighted by the yellow arrows.

Discussion

The viscoelastic MP-FWI case studies presented demonstrate the ability of this approach to generate accurate subsurface models of V_P, V_S/V_P ratio, and P-impedance directly from the raw (or minimally processed) field data. These viscoelastic MP-FWI-derived AVA attributes are geologically conformable and show a good match to the well information. They were also derived without needing to generate reflectivity angle stacks or prestack image gathers for a secondary AVA inversion step because the AVA attributes are obtained directly from viscoelastic MP-FWI. For comparison purposes only, a reflectivity volume was generated from the viscoelastic MP-FWI-derived attributes and assessed against the equivalent result obtained from the conventional workflow involving LS-RTM. The reflectivity derived from viscoelastic MP-FWI also demonstrates notable improvements in resolution over the LS-RTM, further showing that the complex preprocessing stages required by the conventional workflows are no longer required. This simplifies and reduces the subjectivity surrounding the generation of vital QI quantities. The inclusion of multiples, ghosts, and other complex wave phenomena when deriving AVA attributes provides improved illumination and resolution of the subsurface compared to conventional primary-only imaging techniques, resulting in greater understanding of the reservoir location, especially in salt environments.

Another important distinction between the viscoelastic MP-FWI workflow and the conventional workflow is the

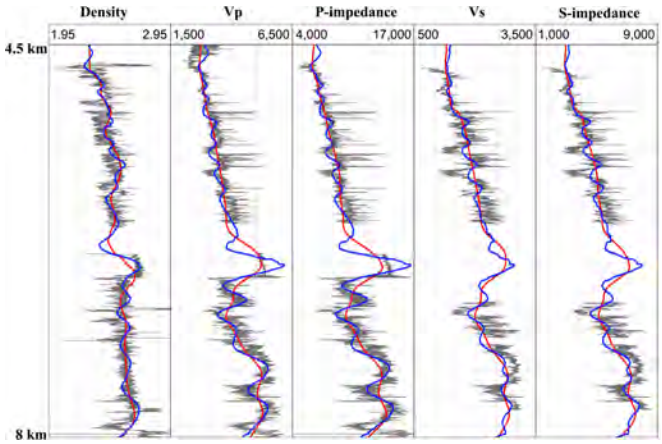

Figure 7. Comparison between the well data (black), initial models (red), and viscoelastic MP-FWI inverted results (blue).

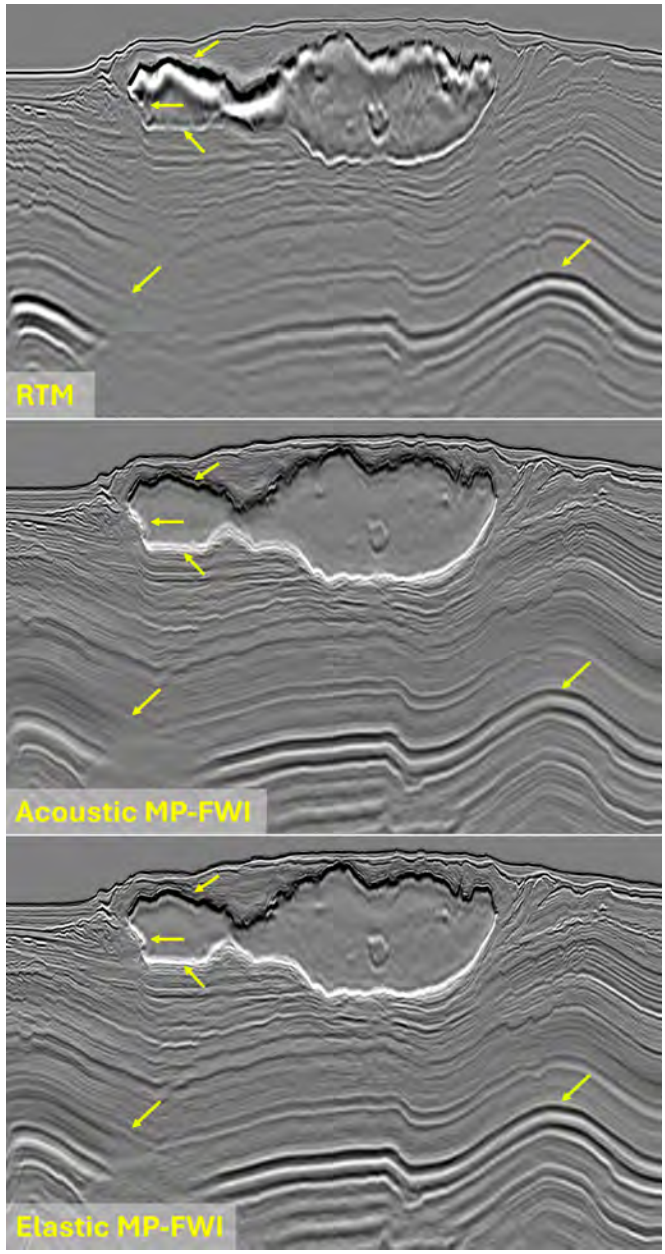

Figure 8. (Top) RTM from conventional approach, (middle) acoustic MP-FWI reflectivity, and (bottom) viscoelastic MP-FWI reflectivity.

inclusion of QI expertise at the beginning of the viscoelastic MP-FWI approach when building the initial models, rather than at the end of the workflow as would be the case with the conventional approach. We do not see the viscoelastic MP-FWI approach serving as a replacement for QI expertise, but rather such expertise is required in building the initial low-wavenumber models at the beginning of the workflow and throughout for QC purposes. Therefore, QI expertise is integrated from the very beginning.

An increasingly important question surrounding AVA-derived attributes from the conventional and viscoelastic MP-FWI approaches is in understanding its uncertainty in a global sense, which describes how much the attributes can be perturbed while still explaining the data equally well. Gaining in-depth knowledge of the feasible error bars associated with the inverted parameters in terms of their physical values and interface depth is critical information for hydrocarbon extraction planning, but often ignored during the imaging or model building stages. Obtaining such information from high-frequency viscoelastic MP-FWI remains costly, with extensive scenario testing currently being uneconomical. Understanding its uncertainty in a local sense, however, offers an attractive alternative for the near future and will form part of future work.

Conclusions

In the two case studies presented, viscoelastic MP-FWI produced geologically conformable models of V_P, V_S/V_P ratio, and P-impedance that match the well information and outperform conventional imaging-derived results in terms of structural interpretability, illumination, and reservoir elastic property estimation.

Incorporating the full wavefield, including multiples and other complex wave phenomena, the viscoelastic MP-FWI approach reduces reliance on the restrictive assumptions and heavy preprocessing demanded by conventional workflows. This enables a simpler and less subjective route to QI while preserving the central role of QI expertise in building and validating the low-wavenumber models.

By using the more complete physics of viscoelastic MP-FWI, the real seismic experiment is replicated in a supercomputer, and it has demonstrated that the conventional four stages of preprocessing, model building, imaging, and AVA inversion can be entirely superseded. TLE

Acknowledgments

The authors thank DUG Technology for permission to publish these results, DUG Multi-Client for permission to use the BEX MC3D data set, and Shell for permission to show the GoM data set. The authors recognize the tremendous efforts of the DUG Wave software team, and the authors thank the Devito Project for their continued efforts.

Data and materials availability

Data associated with this research are confidential and cannot be released.

Corresponding author: jamesm@dug.com

References

Aki, K., and P. G. Richards, 2002, Quantitative seismology. University Science Books: second edition.

Audebert, F., D. Nichols, T. Rekdal, B. Biondi, D. E. Lumley, and H. Urdaneta, 1997, Imaging complex geologic structure with single-arrival Kirchhoff prestack depth migration: Geophysics, **62**, no. 5, 1533–1543, https://doi.org/10.1190/1.1444256.

Baumstein, A., P. Routh, K. Basler-Reeder, Y. H. Cha, D. Tang, J. Barr, and A. Martinez, 2022, Elastic full wavefield inversion: The benefits and the challenges in clastic and subsalt setting: ADIPEC, https://doi.org/10.2118/211620-MS.

Baysal, E., D. D. Kosloff, and J. W. C. Sherwood, 1983, Reverse time migration: Geophysics, **48**, no. 11, 1514–1524, https://doi.org/10.1190/1.1441434.

Bednar, J. B., K. Yoon, C. Shin, and L. Lines, 2003, One way vs two way wave equation imaging — Is two-way worth it? 65th Conference and Exhibition, EAGE, Extended Abstracts, https://doi.org/10.3997/2214-4609-pdb.6.B11.

Bleistein, N., J. W. Stockwell, and J. K. Cohen, 2001, Mathematics of multidimensional seismic imaging, migration, and inversion: Springer.

Gardner, G. H. F., L. W. Gardner, and A. R. Gregory, 1974, Formation velocity and density — The diagnostic basics for stratigraphic traps: Geophysics, **39**, no. 6, 770–780, https://doi.org/10.1190/1.1440465.

Gomes, A., D. Rocha, R. E. Plessix, M. Wong, C. Perkins, and V. Goh, 2025, High-resolution impedance estimation using multi-parameter viscoelastic FWI in a Gulf of Mexico setting: The Leading Edge, **44**, no. 5, 394–402, https://doi.org/10.1190/tle44050394.1.

Guitton, A., 2017, Fast 3D least-squares RTM by preconditioning with nonstationary matching filters, https://doi.org/10.1190/-segam2017-17588457.1.

Hampson, G., 2024, The effects of marine currents on seismic data: Fourth international meeting for applied geoscience & energy, 188–192, https://doi.org/10.1190/image2024-4092216.1.

Hidalgo, C., Ø. Pedersen, and G. Aschjem, 2024, FWI derived angle reflectivity for shallow reservoir seismic characterization in complex imaging areas: 85th EAGE Annual Conference & Exhibition, EAGE, Extended Abstracts, https://doi.org/10.3997/2214-4609.202410651.

Jiang, W., 2020, 3-D joint inversion of seismic waveform and airborne gravity gradiometry data: Geophysical Journal International, **223**, no. 1, 746–764, https://doi.org/10.1093/gji/ggaa296.

Kalinicheva, T., M. Warner, and F. Mancini, 2020, Full-bandwidth FWI: 90th Annual International Meeting, SEG, Expanded Abstracts, 651–655, https://doi.org/10.1190/segam2020-3425522.1.

Köhn, D., A. Kurzmann, A. Przebindowska, D. De Nil, N. Nguyen, and T. Bohlen, 2009, Elastic full waveform tomography of synthetic multicomponent reflection seismic data: Annual Wave Inversion Technology Consortium Meeting, **12**, 106–116.

Liu, H., G. Wu, Q. Li, J. Shan, and S. Yang, 2024, Density prediction from full waveform inversion with gravity gradient constraints:

IEEE Geoscience and Remote Sensing Letters, **21**, 1–5, https://doi.org/10.1109/LGRS.2024.3397889.

Luo, Y., and G. T. Schuster, 1991, Wave-equation traveltime inversion: Geophysics, **56**, 645–653, https://doi.org/10.1190/1.1443081.

Masmoudi, N., A. Ratcliffe, O. Bukola, J. Tickle, and X. Chen, 2024, Elastic FWI of multi-component ocean-bottom seismic to update shear-wave velocity models: 85th EAGE Annual Conference & Exhibition, EAGE, Extended Abstracts, 1–5, https://doi.org/10.3997/2214-4609.202410528.

McLeman, J., T. Rayment, T. Burgess, K. Dancer, G. Hampson, and A. Pauli, 2023, Superior resolution through multiparameter FWI imaging: A new philosophy in seismic processing and imaging: The Leading Edge, **42**, no. 1, 34–43, https://doi.org/10.1190/tle42010034.1.

Nemeth, T., C. Wu, and G. T. Schuster, 1999, Least-squares migration of incomplete reflection data: Geophysics, **64**, no. 1, 208–221, https://doi.org/10.1190/1.1444517.

Pan, W., K. A. Innanen, and Y. Geng, 2018, Elastic full-waveform inversion and parametrization analysis applied to walk-away vertical seismic profile data for unconventional (heavy oil) reservoir characterization: Geophysical Journal International, **213**, no. 3, 1934–1968, https://doi.org/10.1093/gji/ggy087.

Sayers, C. M., and L. D. den Boer, 2011, Rock physics-based relations for density and S-velocity versus P-velocity in deepwater subsalt Gulf of Mexico shales: The Leading Edge, **30**, no. 12, 1376–1381, https://doi.org/10.1190/1.3672482.

Shen, P., U. Albertin, H. Malcotti, and J. Haataja, 2024, Elastic FWI for joint Vp, Vs and density inversion: Fourth international meeting for applied geoscience & energy, 877–881, https://doi.org/10.1190/image2024-4090186.1.

Shen, X., L. Jiang, J. Dellinger, A. Brenders, C. Kumar, M. James, J. Etgen, et al, 2018, High-resolution full-waveform inversion for structural imaging in exploration: 88th Annual International Meeting, SEG, Expanded Abstracts, 1098–1102, https://doi.org/10.1190/segam2018-2997202.1.

Tarantola, A., 1986, A strategy for nonlinear elastic inversion of seismic reflection data: Geophysics, **51**, no. 10, 1893–1903, https://doi.org/10.1190/1.1442046.

Wang, H., O. Burtz, P. Routh, D. Wang, J. Violet, R. Lu, and S. Lazaratos, 2021, Anisotropic 3D elastic full-wavefield inversion to directly estimate elastic properties and its role in interpretation: The Leading Edge, **40**, no. 4, 277–286, https://doi.org/10.1190/tle40040277.1.

Warner, M., J. Armitage, A. Umpleby, N. Shah, H. Debens, and F. Mancini, 2022, Full-elastic AVA extraction using acoustic FWI: Second International Meeting for Applied Geoscience & Energy, Houston, Texas, 907–911, https://doi.org/10.1190/image2022-3750777.1.

Yuan, Y. O., F. J. Simons, and E. Bozdag, 2015, Multiscale adjoint waveform tomography for surface and body waves: Geophysics, **80**, no. 5, R281–R302, https://doi.org/10.1190/geo2014-0461.1.

Zoeppritz, K., 1919, VIIb. Über Reflexion und Durchgang seismischer Wellen durch Unstetigkeitsflächen, [VIIb. On reflection and transmission of seismic waves by surfaces of discontinuity]: Nachrichten von der Königlichen Gesellschaft der Wissenschaften zu Göttingen, Mathematisch-physikalische Klasse, 66–84.